Respiration Effect on Wavelet-Based ECG T-Wave End Delineation Strategies

Maikel Noriega, Juan Pablo Martínez, Pablo Laguna, *Senior Member, IEEE*, Raquel Bailón, and Rute Almeida*

***Abstract*—The main purpose of this paper is to study the influence of the mechanical effect of respiration over the T-wave end delineation. We compared the performance of an automatic delineation system based on the wavelet transform (WT), considering single lead (SL), global delineation locations obtained from SL annotations (SLR), and multilead (ML) approaches. The linear relation between the variations on T-wave end locations obtained with each of the methods and the mechanical effect of respiration was quantified using spectral coherence and ARARX modeling both in simulated signals and in real data. We also explored the evolution of the vectorcardiographic spatial loop using the projection on the main direction of the WT in the region close to the T-wave end (T_e) and its relation with respiration. The dispersion of the additional T-wave end location error due to respiration was reduced by 15% using SLR with respect to SL, while ML allows for a reduction of around 40%. The percentage of that error correlated with respiration was in average 99% using SL while 82% and 72% using SLR and ML, respectively. Thus, results suggest that ML is the most adequate strategy for T-wave delineation, allowing the reduction of the instability of T-wave end location caused by respiration.**

***Index Terms*—Electrocardiogram delineation, respiration, T-wave.**

I. Introduction

THE electrocardiogram (ECG) is a noninvasive and painless procedure and an essential diagnostic tool for many cardiac and noncardiac conditions. Each heart beat is produced by an electric wavefront that crosses the different cardiac structures; the activation/inactivation of those is reflected in different ECG waves (P, Q, R, S, T) which can be used to infer both wave durations and beat-to-beat variations (see Fig. 1). The time intervals defined by the waves' onsets, peaks, and ends are clinically relevant [1], [2], as it is the case of the RR interval (measured between consecutive R-waves) used as standard for cycle duration and to calculate heart rate (HR).

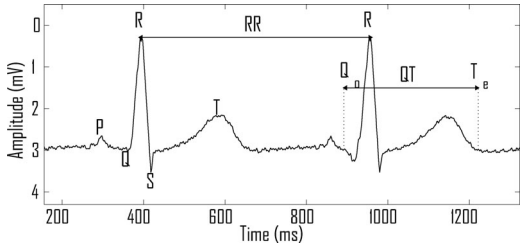

Fig. 1. Principal waves of a beat and RR and QT intervals. The R peak mark locates the beat and the marks of the onset of the QRS (Q_o) and of the T-wave end (T_e) correspond, respectively, to the onset and end of the ventricular activity (depolarization and repolarization process).

In particular, the T-wave end (T_e) timing corresponds to the end of the ventricular activity and its correct location is required by many strategies used for ventricular repolarization (VR) analysis. Both the QT, measured from the onset of the QRS complex (Q_o) to the T_e, and the RT, measured from the R peak to the T_e, intervals have been used as indeces of the VR time [3], [4]. Abnormal QT values, as well as prolongation of the time interval from the T-wave peak to the T_e, have been associated with ventricular pro-arrhythmicity and sudden cardiac death [2]. Moreover the study of possible effects over the QT is mandatory to guaranty the cardiac safety of any drug, prior to its commercialization [5]–[7]. The dispersion of the VR, measured as beat-to-beat variations and by the normalized QT variability index (QTVI = log ratio between the QT and HR variabilities, each normalized by its square mean) have been repeatedly reported as risk stratifiers and associated with life-threatening arrhythmia and sudden death [8]–[10]. Therefore, the correct location of the T_e provides a fundamental feature to derive clinically useful information. The stability of the automatic mark, avoiding spurious beat-to-beat variability resulting from non cardiac sources, is of extreme importance. Locating accurately the T_e can be particularly difficult in the case of smooth T-waves with low SNR. Nevertheless, there is a lack of gold standard for T_e location and developing a consensus definition remains a challenge [6], [7].

By using several electrodes it is possible to access simultaneous *electrocardiographic leads*, providing a spatial perspective

Manuscript received November 16, 2011; revised April 9, 2011; accepted May 2, 2011. Date of publication May 27, 2011; date of current version June 20, 2012. This work was supported in part by the MCyT and FEDER under Project TEC2010-21703-C03-02, by Grupo Consolidado Communications Technology Group (GTC) from DGA T:30 and in part by the grants from the Banco Santander Central Hispano and University of Zaragoza. Centro de Investigación Biomédica en Red en Bioingeniería, Biomateriales y Nanomedicina is an initiative supported in part by the VI National R&D&i Plan 2008–2011, Iniciativa Ingenio 2010, Consolider Program, CIBER Actions and in part by the Instituto de Salud Carlos III with assistance from the European Regional Development Fund. Centro de Matemática da Universidade do Porto (CMUP) is supported by Fundação para a Ciência e a Tecnologia (FCT), Portugal, through POCI2010/POCTI/POSI programmes, with national and European Community Structural Funds. *Asterisk indicates corresponding author.*

M. Noriega is with the Communications and Electronical Department of Oriente University, Santiago de Cuba 90400, Cuba, and also with Communications Technology Group, Aragón Institute of Engineering Research, IIS Aragón, University of Zaragoza, Zarogaza 50001-50018, Spain and Centro de Investigación Biomédica en Red en Bioingeniería, Biomateriales y Nanomedicina, Zaragoza 50001-50018, Spain (e-mail: mnoriega@unizar.es).

J. P. Martínez, P. Laguna, and R. Bailón are with the Communications Technology Group, I3A, IIS Aragón, UZ, and also with Centro de Investigación Biomédica en Red en Bioingeniería, Biomateriales y Nanomedicina, Zaragoza 50001-50018, Spain (e-mail: jpmart@unizar.es; rbailon@unizar.es; laguna@unizar.es).

*R. Almeida is with the Centro de Investigación Biomédica en Red en Bioingeniería, Biomateriales y Nanomedicina, Zaragoza 50001-50018, Spain, with the Communications Technology Group, I3A, IIS Aragón, UZ, Zaragoza 50001-50018, Spain and also with the CMUP, 4169-007 Porto, Portugal (e-mail: rbalmeid@unizar.es, rbalmeid@fc.up.pt).

Digital Object Identifier 10.1109/TBME.2011.2157824

0018-9294/$31.00 © 2012 IEEE

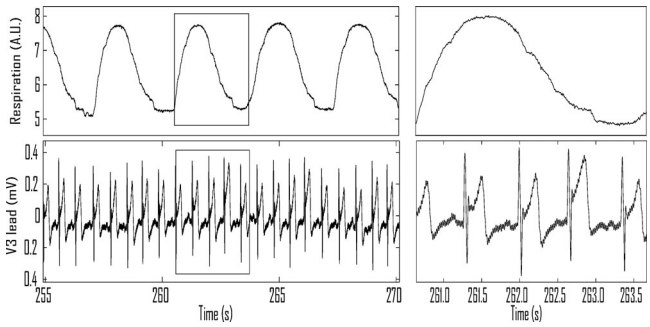

Fig. 2. Example of morphology changes of the ECG signal caused by respiration. On the right there is a zoom of the area inside the rectangle.

of the heart's electrical activity [1], [11]. The cardiac dipole model approximates the electrical activity from the heart by a time-variant electrical dipole called electric heart vector (EHV) [11]. According to this model, each lead can be interpreted as the projection of the EHV over the vector that defines the lead direction. The EHV's canonical representation is given by the vectorcardiogram (VCG) defined by 3 orthogonal leads $[x(n), y(n), z(n)]$, usually acquired as the corrected Frank leads. The exact timing in which the VR is over cannot be systematically determined by a particular ECG lead. The correspondent projection of the T-wave loop in the VCG depends on the loop orientation with respect to the given lead, as influenced by the cardiac electrical axis, which can vary due to chest movements (respiration) and other physiological processes [12].

Respiration influences the ECG in various ways. During the respiratory cycle, chest movements, and changes in the thorax impedance distribution due to filling and emptying of the lungs cause a rotation of the electrical axis of the heart which has an effect over beat morphology [13], [14] (see Fig. 2). This effect is referred to as the mechanical effect of respiration on the ECG. Nevertheless, respiration modulates HR, and therefor RT and QT intervals, such that it increases during inspiration and decreases during expiration. This is denoted to as the autonomic effect, as it is mainly due to the control of the autonomic nervous system (ANS) [15], in spite of evidence that it may also have a mechanical origin.

The effect of respiration on ECG morphology, as result of the changes on the VCG loop orientation with respect to the projection axis, is likely to cause errors or instabilities in automatic delineation. In [16] Sörnmo proposed a method to align the VCG loops before performing morphologic beat-to-beat variability in order to cope with the spurious effects. In [17], we found that a multilead (ML) delineation strategy that estimates the VCG loop main direction and uses the projection over it to locate the T_e, allows us to increase the stability of the QT interval measurement, with respect to using single-lead (SL) delineation or postprocessing rules after SL delineation (SLR) in real multilead ECG signals. We hypothesize that this is a consequence of a lower influence of the mechanical effect of respiration over ML-based automatic locations by the adjustment of the projection axis, compensating the changes over the loop orientation. To validate this hypothesis, in this paper we performed a simulation study in which the respiratory effect over the delineation of T_e is assessed. We also investigate in real signals whether the mechanical influence of respiratory activity on the ECG is reflected on the several delineation strategies and how it influences over the stability of the obtained marks. Our main goal is to provide evidences that, among T-wave end delineation strategies, the ML achieves the maximum reduction of the mechanically driven spurious variability of the delineation error by compensating the respiratory mechanical effect over the ECG, and to extract useful information on this process to further improve the delineation in the future. In doing so we will establish that this should be the preferred strategy for QT variability analysis, and the basis for further improvements in delineators.

II. Materials and Methods

There are several published methodologies for automatic ECG delineation. Particularly in this paper we discuss the multiscale wavelet transform (WT)-based delineator previously described and validated in [18] and [19]. Notation can be found in Appendix.

A. Automatic Delineation

1) SL and SLR for Multilead Signals: For each lead, a set of differentiated signals, smoothed at different scales, is obtained by means of the discrete WT, using a quadratic spline as prototype wavelet [18]. First, detection and classification of waveforms are performed by searching for the maxima and minima at different scales. Then, the ECG boundaries [20] are located using a threshold approach across scales. This allows us to obtain a set of annotations for each available lead [18]. This SL approach has the limitation that the electrical cardiac activity is a global phenomena and therefore it is desirable to consider an approach in which all ECG leads are taken into account to produce global marks.

One strategy for dealing with multilead signals is the inclusion of postprocessing rules (SLR) after the SL-based delineation. This consists in obtaining a global mark constructed or chosen from the marks given by each lead. A simple rule is to choose the median (more robust with respect to outliers compared with arithmetic mean) of the SL marks as the peak of the wave. The mark for a wave's onset (end) should be the earliest (latest) one, with some outliers protection [21]. These rules perform properly as long as they have a large set of leads available (for instance on a record acquired according to the standard 12-lead system) but are hardly adequate for a record with just 2 or 3 leads (e.g., Frank leads on a VCG record).

2) ML Delineation: Although the SLR strategy finally gives one single mark per boundary or peak, it does not use all available spatial information. The ML delineation departs from the SL but considers simultaneously the orthogonal leads of the VCG [19]. Denoting by $w_{s,m}(n)$ the WT of a signal $s(n) \in \{x(n), y(n), z(n)\}$ in the scale m, for a VCG loop given by $[x(n), y(n), z(n)]^T$, the correspondent spatial WT loop is defined as

$$\mathbf{w}_m(n) = [w_{x,m}(n), w_{y,m}(n), w_{z,m}(n)]^T. \quad (1)$$

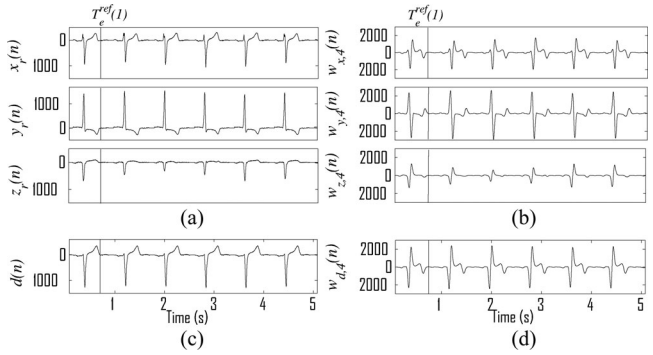

Fig. 3. Example of derived $d(n)$ and $w_{d,4}(n)$ signal. (a) Leads $x_r(n)$, $y_r(n)$, and $z_r(n)$ of VCG signal (μV) correspond to simulated sinal affected by respiration (see Section II-B1). (b) WT of leads $x_r(n)$, $y_r(n)$, and $z_r(n)$ in scale 4 (A.U.). (c) Derived ECG lead ($d(n)$) (μV). (d) Derived WT ($w_{d,4}(n)$) signal (A.U.). Vertical line corresponds to T_e.

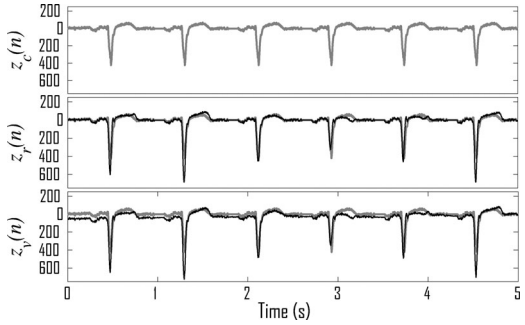

Fig. 4. Example of artificial ECG signals in lead Z: clean ECG signal $z_c(n)$ (μV) segment (plotted in gray in all axis for comparative purposes), same segment as in $z_c(n)$ (μV) but with respiration effect for $F_r = 0.27$ Hz ($z_r(n)$) and with noise contamination for $\mathrm{SNR} \in \{15\}$ dB ($z_v(n)$).

As a consequence of the derivative nature of the WT prototype used, the WT loop $\mathbf{w}_m(n), n \in L$, is proportional to the smoothed VCG derivative [22] and describes the velocity of evolution of the EHV in a time interval L. Assuming that the noise is spatially homogeneous, the direction with maximum projection of the WT in the region close to the wave boundary would define the ECG lead maximizing the local SNR, and thus, the most appropriate for the boundary delineation. The main direction $\mathbf{u} = [\mathrm{u}_x, \mathrm{u}_y, \mathrm{u}_z]^T$ of EHV variations on any time interval L is given by the directions of the best straight linear fit to all points in the WT loop. By choosing adequately the time interval L, around the fiducial point of interest, it is possible to find direction $\mathbf{u}$ corresponding to the lead most suited for delineation purposes [19].

The projection of the VCG loop $[x(n), y(n), z(n)]^T$ over the direction $\mathbf{u}$ produces a derived lead $d(n)$. Projecting the WT loop $\mathbf{w}_m(n)$ over $\mathbf{u}$ allows us to obtain a *derived wavelet* lead $w_{d,m}(n)$ that combines the information provided by the three VCG leads

$$w_{d,m}(n) = \frac{\mathbf{w}_m^T(n) \cdot \mathbf{u}}{\|\mathbf{u}\|} \quad n \in I \tag{2}$$

It should be noted that the time intervals I (used for projecting) and L (used for linear fitting) can be different, depending on each wave specificities.

The ML boundary delineation strategy using WT loops is based on a multistep iterative search for *final* direction $\mathbf{u}$ producing a better spatial lead (with *steeper* slopes) for each boundary delineation. The goal is to construct a *derived wavelet* signal well suited for boundaries location, using the same detection criteria as in the SL delineator [19]. In Fig. 3, we show an example of the derived ECG lead optimal for T-wave end delineation and WT signal from the combination of the information provided by the three VCG leads.

B. Data

1) Simulation Data: To validate our hypothesis, we constructed artificial ECG signals based on the method described in [3]. Short segments of artificial ECG are plotted in Fig. 4.

Clean ECG simulation: An artificial 3-lead clean ECG signal $[x_c(n), y_c(n), z_c(n)]^T$ was constructed by concatenation of 100 stretched versions of a real template beat sampled at 500 Hz, following $\mathrm{RR}(i)$ and $\mathrm{QT}(i)$ series extracted from a real record of the PTB database [23], where *i* is the beat number. The template beat (without apparent noise), chosen from a 12-lead ECG, and the Frank leads were synthesized using the inverse *Dower* transformation [24]. SL delineation of the template beat was used to obtain the locations of the R peak, the QRS complex onset/end and the T_e. The reference mark for the R peak was taken from the three SL marks as the one corresponding to the largest signal amplitude, while for the boundaries the earliest/latest SL marks for the onset/end were taken.

To reflect the variability inherent to the corresponding clean series $\mathrm{QT}(i)$, the template beat was properly stretched from the QRS end to the T_e reference mark, to produce the target QT interval. By applying the same stretching to each orthogonal lead, an artificial 3-lead ECG signal with the same variability in all leads and known T_e locations $T_e^{\mathrm{ref}}(i)$ is obtained [3]. The stretched beats were then concatenated following the target RR series.

Respiration effect: The mechanical effect of respiration was simulated over the artificial ECG signals as a cardiac electrical axis rotation, in the same way as in [3]. The signals affected by respiration $[x_r(n), y_r(n), z_r(n)]^T$ displayed in Fig. 3(a) were constructed from $[x_c(n), y_c(n), z_c(n)]^T$ by introducing an effect equivalent to pure sinusoidal respiration at a frequency F_r modeled as a rotation, with a maximum angle ϕ rad, around the three orthogonal axes. First $F_r \in \{0.15, 0.20, 0.25, 0.27, 0.30, 0.35, 0.40\}$ Hz and $\phi = 15^{\mathrm{o}}$ were considered [25], [26]. Note that $F_r = 0.27$ Hz corresponds to the real respiratory frequency associated with the QT*(i)* and RR*(i)* series used to construct the simulated signal and that the rotation angle $\phi = 15^{\mathrm{o}}$, corresponds to a large physiological respiration related rotation angle. Then, different maximum rotation angles ($\phi \in \{5^{\mathrm{o}}, 10^{\mathrm{o}}, 15^{\mathrm{o}}\}$) were considered for $F_r = 0.27$ Hz.

Noise contamination: Noise contamination was included in the simulation study by adding noise records to $[x_r(n), y_r(n), z_r(n)]^T$. Noise records were obtained by

subtracting an exponentially updated average beat from a real stress testing ECG and rejecting afterward the residual QRS peaks [27]. Then the inverse Dower transformation is applied to obtain the 3-lead noise signal $[v_x(n), v_y(n), v_z(n)]^T$. The three noise leads were rescaled by a constant a to get a $\mathrm{SNR} \in \{30, 25, 20, 15, 10\}$ dB:

$$a = \left(\frac{P_{x_r} + P_{y_r} + P_{z_r}}{P_{v_x} + P_{v_y} + P_{v_z}} \cdot 10^{\frac{-\mathrm{SNR}}{10}} \right)^{\frac{1}{2}} \tag{3}$$

were P_s denotes the power of signal $s(n)$. The noise was added to the ECG signal with respiratory effect corresponding to $F_r = 0.27$ Hz and $\phi = 15^{\mathrm{o}}$, obtaining the noisy signal $[x_v(n), y_v(n), z_v(n)]^T$.

2) Real Data: To extend the study to real signals we analyzed two databases: the PTB database and a database of ECG signals from healthy subjects recorded at University of Zaragoza, Zaragoza, Spain, which we call control database (CDB).

PTB database [23]: We use the 60 control recordings included in these databases, each one containing the 12-standard and 3-Frank lead ECG, sampled at 1000 Hz.

CDB database: This database contains the standard 12-lead ECG and a respiration signal $(r(n))$ of 40 subjects (age 32 $\pm$ 9 years, 26 male/14 female), recorded during 5 min of supine resting and all were here considered. The MP 150 (BIOPAC Systems) was used to acquire simultaneously the ECG (ECG100C amplifier and disposable Ag–AgCl electrodes) at a sampling frequency of 1000 Hz, and the respiration signal (RSP100C and a strain gauge transducer) at a sampling frequency of 125 Hz.

The ECG signals were delineated using the SLR and ML delineation strategies. The ML strategy in PTB database was applied over Frank leads while in CDB over the three leads obtained with inverse Dower's transformation. SLR delineation was applied over the 12 standard leads in both databases; $RT_e^M(i)$ interval was measured from the R peak obtained with SLR to $T_e(i)$ for each delineation system $M \in \{\mathrm{SLR}, \mathrm{ML}\}$. The mechanical effect of respiration was estimated from the ECG signal in the two databases using the algorithm proposed in [26]. In this method, the ECG-derived respiratory (EDR) signal is estimated from the VCG as the series of rotation angles around each orthogonal lead ($\varphi_x(i), \varphi_y(i)$ and $\varphi_z(i)$), estimated between successive QRS–VCG loops and a reference QRS–VCG loop by least-squares minimization.

C. Performance Indexes

1) Simulation Data: The clean (c), respiration affected (r), and noise contaminated (v) simulated ECG signals, were delineated with SL (over lead X), SLR, and ML to obtain the marks $T_e^{\mathrm{M,s}}(i)$, $M \in \{\mathrm{SL}, \mathrm{SLR}, \mathrm{ML}\}$ and $s \in \{c, r, v\}$. For SLR delineation the Dower's transformation was applied to obtain the 12 standard leads [24].

The delineation error was calculated as the difference between the marks found over the ECG and the reference marks used in the simulation:

$$e_{\mathrm{M}}^s(i) = T_e^{\mathrm{M,s}}(i) - T_e^{\mathrm{ref}}(i). \tag{4}$$

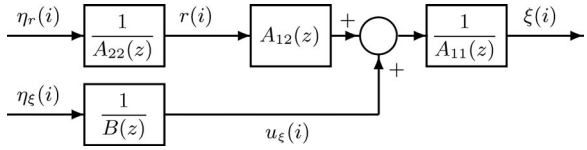

Fig. 5. Model of $\xi(i)$ and $r(i)$ interactions.

Expression (4) can be rewrite as

$$\begin{aligned} e_{\mathrm{M}}^s(i) &= (T_e^{\mathrm{M,s}}(i) - T_e^{\mathrm{M,c}}(i)) + (T_e^{\mathrm{M,c}}(i) - T_e^{\mathrm{ref}}(i)) \\ &= \mathcal{E}_{\mathrm{M}}^s(i) + e_{\mathrm{M}}^c(i) \end{aligned} \tag{5}$$

where $e_{\mathrm{M}}^c(i)$ is the delineation error in the clean signal, and $\mathcal{E}_{\mathrm{M}}^s(i)$ is the additional error due to respiration or noise. In this paper, we will focus on the study of the relation of this additional error $\mathcal{E}_{\mathrm{M}}^s(i)$ with the mechanical effect of respiration. The linear relation between the respiratory signal $(r(n))$ and series of $e_{\mathrm{M}}^r(i), e_{\mathrm{M}}^v(i), \mathcal{E}_{\mathrm{M}}^r(i)$ or $\mathcal{E}_{\mathrm{M}}^v(i)$ was measured using both a nonparametric (spectral coherence) and a parametric method (ARARX modeling).

The spectral coherence was calculated after resampling at 5 Hz the respective series obtaining $\mathcal{E}_{\mathrm{M}}^s(n), s \in \{r, v\}$ and the $r(n)$. To evaluate the relation between $r(n)$ and the *final* direction $\mathbf{u}$, for both cases in which respiratory mechanical effect was introduced, the angles of $\mathbf{u}$ with respect to the plane defined by each pair of orthogonal leads were obtained, $\angle_\rho^r(i)$ and $\angle_\rho^v(i); \rho \in \{(x, y), (y, z), (x, z)\}$, corresponding respectively to the angles with respect to the frontal, sagittal, and transversal planes of the human body. Additionally, the spectral coherences between $r(n)$ and the resampled angles, $\angle_\rho^r(n)$ and $\angle_\rho^v(n)$, were also obtained. The average value of the spectral coherence was computed in a band centered on F_r and with a bandwidth of 0.04 Hz and denoted as $C_{r,\mathcal{E}_{\mathrm{M}}^s}$ for the differences $\mathcal{E}_{\mathrm{M}}^s(n)$ and $C_{r,\angle_\rho^s}$ for the angles.

An open-loop ARARX model [4], schematically presented in Fig. 5, was also used to explore the linear relation between the respiration $r(i)$ and the time series of interest $\xi(i) = \mathcal{E}_{\mathrm{M}}^s(i), s \in \{r,\ v\}$. This parametric methodology allows us to quantify the fraction of variability which results from the mechanical influence of respiration. The series $\eta_r(i)$ and $\eta_\xi(i)$ are mutually uncorrelated stationary zero mean white gaussian processes, with standard deviation (SDs) λ_r and λ_ξ. $A_{11}(z)$, $A_{12}(z)$, $A_{22}(z)$, and $B(z)$ are polynomials with coefficients $a_{11}(k), a_{12}(k), a_{22}(k)$, and $b(k)$, respectively. In the simulation study the series $r(i)$ were obtained by sampling the respiratory signal $r(n)$ at the beat instant $r(i) = r(n)|_{n=i\mathrm{th\ QRS\ beat\ sample}}$ and are modeled as an order $p = 2$ autoregressive stationary random process:

$$r(i) = -\sum_{k=1}^{2} a_{22}(k) r(i-k) + \eta_r(i). \tag{6}$$

The $\xi(i)$ trend is assumed to result from two uncorrelated sources, one driven by $r(i)$ and another resulting from an AR

process with a white noise input $\eta_\xi(i)$. That is

$$\xi(i) = \sum_{k=0}^{q} a_{12}(k) r(i-k) + u_\xi(i) - \sum_{k=1}^{q} a_{11}(k)\xi(i-k)$$

$$u_\xi(i) = -\sum_{k=1}^{q} b(k) u_\xi(i-k) + \eta_\xi(i) \tag{7}$$

where values $q = 2, 3, 4, 5, 6$. For simplicity, the same order q was assumed for all ARARX model polynomials.

ARARX model parameters were iteratively obtained using the generalized least-squares (GLS) method [28]. The order q is taken as the one minimizing the multivariate AIC $\log(\det(\mathbf{\Sigma})) + 2 * (p + 3q + 1)/N$, where $\det(\mathbf{\Sigma})$ stands for the determinant of the covariance matrix of the residuals [$\eta_r(i)$ and $\eta_\xi(i)$] and N is the number of intervals (beats) in the segment. Note that as $p = 2$ is fixed and the $\eta_r(i)$ variance have been already determined in the previous step, only the q order remains to be chosen and this is not a multivariate minimization in strict sense.

The assumption of uncorrelated sources allows us to compute the power spectral density (PSD) functions of each $\xi(i)$ as the sum of two partial spectra: $\mathcal{S}_\xi(F) = \mathcal{S}_{\xi|r}(F) + \mathcal{S}_{\xi|\xi}(F)$:

$$\mathcal{S}_{\xi|r}(F) = T_R \lambda_r^2 \left| \frac{A_{12}(z)}{A_{11}(z)A_{22}(z)} \right|^2_{z=e^{j2\pi F T_R}}$$

$$\mathcal{S}_{\xi|\xi}(F) = T_R \lambda_\xi^2 \left| \frac{1}{A_{11}(z)B(z)} \right|^2_{z=e^{j2\pi F T_R}} \tag{8}$$

where T_R stands for the mean of the $RR(i)$ in the analyzed segment.

The power for each PSD in the frequency band of interest HF (0.15–0.4 Hz), corresponding to the respiration frequency band ($P_{\xi|r}, P_{\xi|\xi}$) is calculated by decomposing these spectra and summing the contributions of the poles in the band:

$$R_{\xi|r} = \frac{P_{\xi|r}}{P_{\xi|r} + P_{\xi|\xi}} \times 100 \tag{9}$$

represents the relative fraction of $\xi(i)$ variability driven by $r(i)$.

2) Real Data: The delineation error in real ECG signals cannot be calculated, as there is no reference T_e mark. Instead, the differences between the automatic T_e locations obtained using the two strategies were calculated:

$$\Delta T_e(i) = T_e^{\mathrm{SLR}}(i) - T_e^{\mathrm{ML}}(i) \tag{10}$$

For the ML strategy we also obtained the angles of the *final* direction $\mathbf{u}$ with respect to the frontal, sagittal and transversal planes of the human body, defined by each pair of orthogonal leads ($\angle_\rho; \rho \in \{(y,z),(x,z),(x,y)\}$, respectively). The linear relation between $\varphi_l(i), l \in \{x,y,z\}$ and $\Delta T_e(i)$, $RT_e^{\mathrm{M}}(i)$ or $\angle_\rho(i)$ was measured using both the nonparametric and parametric approaches as described for the simulated data cases. Thus, the spectral coherences $C_{r,d}; d \in \{\Delta T_e, RT_e^{\mathrm{M}}, \angle_\rho\}$ were obtained by computing the mean value in a band centered on the respiratory frequency, estimated from $\varphi_l(i)$, with a bandwidth of 0.04 Hz. Also, the ARARX model was applied to obtain the relative fraction of $\xi(i) = \Delta T_e(i), RT_e^{\mathrm{M}}(i), \angle_\rho(i)$ variabilities linearly explained by the respiration $r(i)$, according to (8). $r(i)$ is taken either as $\varphi_l(i)$ or as the resampled respiratory signal $r(n)$, when it is available as in the CDB.

TABLE I
MEAN ± SD OF $\mathcal{E}_{\mathrm{M}}^r(i)$ AND e_{M}^c FOR DIFFERENT F_r AND ϕ

F_r (Hz)	ϕ (degrees)	$\mathcal{E}_{\mathrm{SL}}^r$ (ms)	$\mathcal{E}_{\mathrm{SLR}}^r$ (ms)	$\mathcal{E}_{\mathrm{ML}}^r$ (ms)
0.15	15	-5.48 ± 4.2	-0.26 ± 3.6	-1.24 ± 1.9
0.20	15	-5.52 ± 4.2	-0.10 ± 3.5	-1.44 ± 2.0
0.25	15	-5.56 ± 4.3	-0.22 ± 3.6	-1.06 ± 1.9
0.27	15	-5.60 ± 4.3	-0.18 ± 4.0	-1.02 ± 2.1
0.30	15	-5.48 ± 4.3	-0.14 ± 3.6	-1.18 ± 2.1
0.35	15	-5.56 ± 4.2	-0.30 ± 3.5	-1.18 ± 1.9
0.40	15	-5.52 ± 4.2	-0.08 ± 3.8	-1.20 ± 2.0
0.27	5	-1.84 ± 1.6	-0.24 ± 3.9	0.12 ± 1.5
0.27	10	-3.68 ± 2.9	-0.18 ± 4.0	-0.58 ± 1.7
–	–	e_{SL}^c (ms)	e_{SLR}^c (ms)	e_{ML}^c (ms)
		-25.56 ± 1.3	9.18 ± 3.3	-3.20 ± 1.3

III. RESULTS

A. Simulation Study

The mean ± SD of $\mathcal{E}_{\mathrm{M}}^r(i)$ for different values of F_r and ϕ are presented in Table I. Last row shows mean ± SD for the delineation errors $e_{\mathrm{M}}^c(i)$ over the clean simulated data. In Fig. 6(a) and (b) are presented the distributions of the errors $e_{\mathrm{M}}^c(i)$ and $e_{\mathrm{M}}^s(i)$, and of the differences $\mathcal{E}_{\mathrm{M}}^r(i)$, considering simulated respiration with different values of F_r and ϕ. In general, ML delineation outperforms SL and SLR (lower error bias and dispersion). As expected, both bias and variability of the errors increased with the inclusion of respiration, but ML delineation is less affected than SL or SLR. The performance decreases most for the higher maximum rotation angle $\phi = 15^{\mathrm{o}}$, with similar results for the several F_r values considered. The additional error due to respiration $\mathcal{E}_{\mathrm{M}}^r(i)$ for the maximum ϕ represents roughly the fifth part of the total error using SL and more than half of the total error using ML. Moreover, the dispersion of the $\mathcal{E}_{\mathrm{M}}^r(i)$ is comparable or higher than the error dispersion itself. Note also that using ML the dispersion of $\mathcal{E}_{\mathrm{M}}^r(i)$ becomes lower than using SL or SLR, for all combinations. In particular for $\phi = 5^{\mathrm{o}}$ the $\mathcal{E}_{\mathrm{ML}}^r(i)$ are almost equal to 0.

Fig. 7 shows the delineation errors $e_{\mathrm{M}}^s(i)$ and the correspondent simulated $r(i)$ and $\mathcal{E}_{\mathrm{M}}^r(i)$ found using each delineation strategy over the clean simulated signal and considering $F_r = 0.27$Hz and $\phi = 15^{\mathrm{o}}$. The increased variability of $e_{\mathrm{SLR}}^c(i)$ compared with $e_{\mathrm{SL}}^c(i)$ is caused by the protection rules of SLR which changes the lead chosen by the rules. The resemblance between $r(i)$ and $e_{\mathrm{SL}}^r(i)$ and $\mathcal{E}_{\mathrm{SL}}^r(i)$ is remarkable, with a clear periodic component corresponding to F_r. This component can also be seen in $\mathcal{E}_{\mathrm{SLR}}^r(i)$, but is less evident. Similar results were obtained for other values of F_r and ϕ. In Fig. 8(b) the results of both nonparametric ($C_{r,\mathcal{E}_M^r}$) and parametric ($R_{\xi|r}^r$) methodologies to measure the linear relation between $r(n)$ and $\mathcal{E}_{\mathrm{M}}^r(i)$ are presented. Note that both the average coherence values and the relative fraction of the HF variability of $\mathcal{E}_{\mathrm{M}}^s(i)$ explained by $r(i)$ obtained with SL are higher than those obtained with ML and SLR for all F_r considered. This indicates that the additional

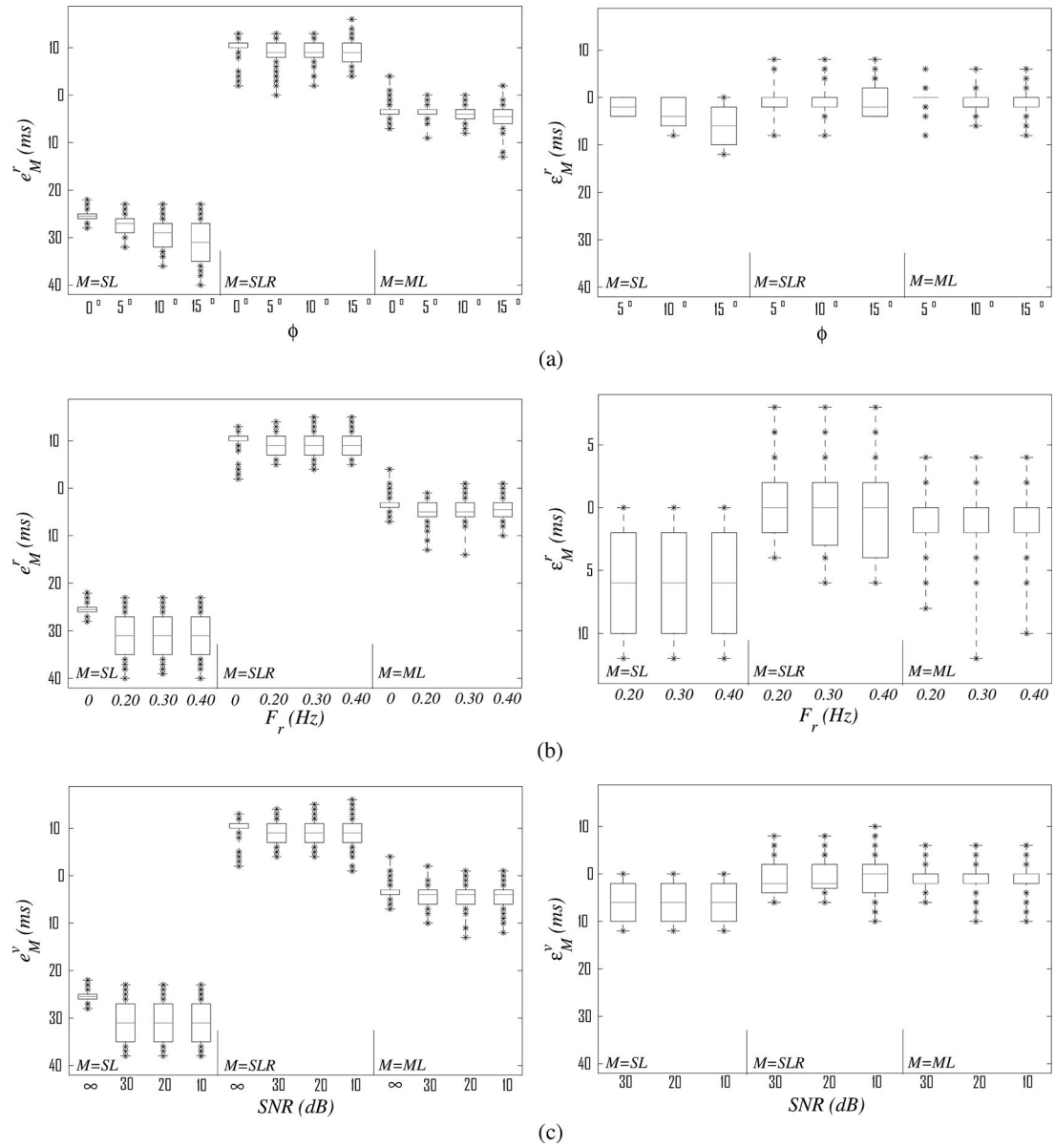

Fig. 6. Distributions of the errors $e^s_{\mathrm{M}}(i)$ and differences $\mathcal{E}^s_{\mathrm{M}}(i)$, considering simulated respiration with different values of F_r and ϕ and simulated noise with different SNR values. $F_r = 0$ Hz or $\phi = 0^\circ$ stands for clean simulated signal and $\mathrm{SNR} = \infty$ stands for no simulated noise included. (a) $\phi \in \{0^\circ, 5^\circ, 10^\circ, 15^\circ\}$, $F_r = 0.27$, $\mathrm{SNR} = \infty$. (b) $\phi = 15^\circ$, $F_r \in \{0, 0.20, 0.30, 0.40\}$ Hz, $\mathrm{SNR} = \infty$. (c) $F_r = 0.27$, $\phi = 15^\circ$, $\mathrm{SNR} \in \{0, 30, 20, 10\}$ dB.

error in the T_e marks obtained by SL delineation is more linearly related to the mechanical effect of respiration.

The mean and SD values of $\mathcal{E}^v_{\mathrm{M}}$ are shown in Table II and the distributions of the errors $e^v_{\mathrm{M}}(i)$ and differences $\mathcal{E}^v_{\mathrm{M}}(i)$ are presented in Fig. 6(c) for several SLR values. In the presence of noise there is no relevant performance decrease for none of the delineation approaches. The additional error with respect to clean simulated signal remains similar to the case with and no noise inclusion ($\mathrm{SNR} = \infty$). In Fig. 8(b) the values obtained for $C_{r,\mathcal{E}^V_M}$ and $R^V_{\xi|r}$ are presented. The level of linear relation between $r(n)$ and $\mathcal{E}^v_{\mathrm{M}}(i)$ is similar than for case with the same F_r value and $\mathrm{SNR} = \infty$. A lower relation is found using ML than with SL or SLR, confirming a weaker influence of the mechanical respiration over the delineation error.

In order to explain the apparent robustness of ML to the mechanical effect of the respiration we explore the main directions $\mathbf{u} = [\mathrm{u}_x, \mathrm{u}_y, \mathrm{u}_z]^T$ of EHV variations found by ML for T_e delineation. Fig. 9 display the u_x, u_y, and u_z found over clean simulated signal and for the cases of $F_r = 0.27$, $\phi = 15^{\mathrm{o}}$ with no noise included and with $\mathrm{SNR} \in \{30, 10\}$ dB. While for clean signal the *final* direction $\mathbf{u}$ is quite stable across beats, for all cases with respiratory effect a periodic component corresponding to F_r value is visible for all coordinates. Analyzing the average coherence values between $r(n)$ and the angles $\angle^r_\rho(n)$ and $\angle^v_\rho(n)$ and the relative fractions of $\mathcal{E}^s_{\mathrm{M}}(n)$ variability explained by those angles (see Fig. 10) we can confirm a strong linear relation between the *final* direction $\mathbf{u}$ and $r(n)$ for all cases.

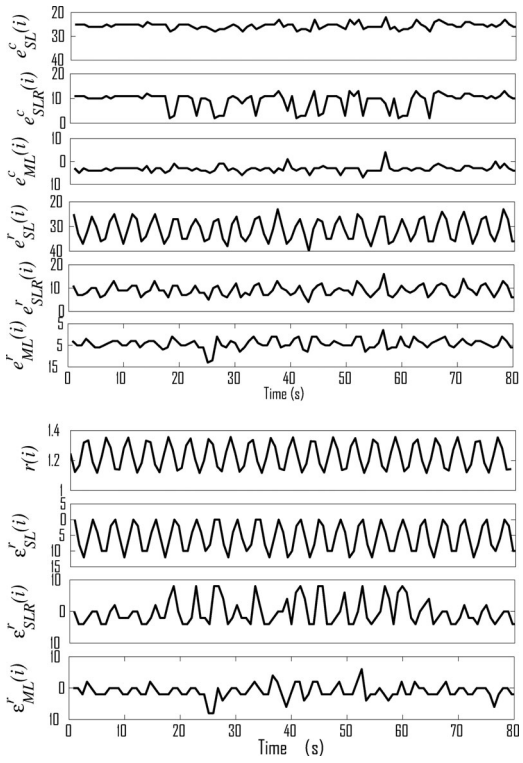

Fig. 7. Delineation errors and additional error (ms) due to respiration found in the simulation study using several delineation approaches.

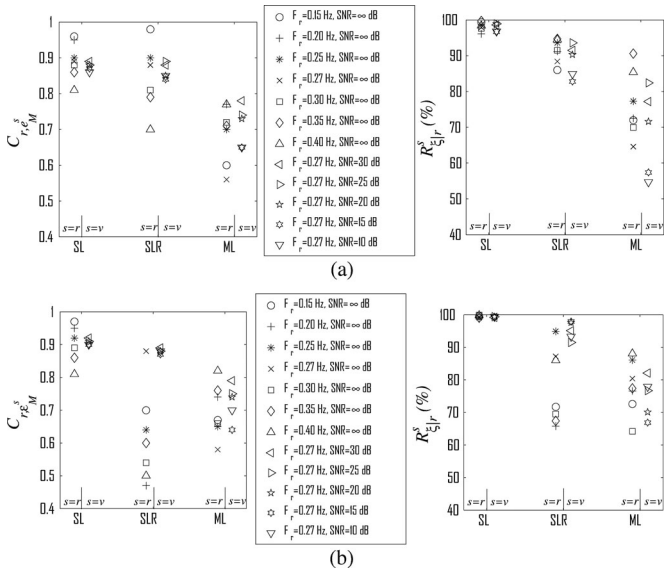

Fig. 8. Average coherence values and relative fractions of the total delineation error or additional error including the respiration. $\mathrm{SNR} = \infty$ stands for no simulated noise included. (a) Linear relation between $r(n)$ and $e^r_{\mathrm{M}}(i)$ or $e^v_{\mathrm{M}}(i)$. (b) Linear relation between $r(n)$ and $\mathcal{E}^r_{\mathrm{M}}(i)$ or $\mathcal{E}^v_{\mathrm{M}}(i)$.

B. Real ECG Study

The linear relation between the estimated $\varphi_x(i)$ and $RT^{\mathrm{M}}_e(i)$ or $\Delta T_e(i)$ found in the PTB database are shown in Fig. 11 as the average coherence values $C_{r,d}$ (nonparametric method) and fraction of variability $R_{\xi|r}$ explained by $\varphi_x(i)$ (parametric method). It can be observed that a strong relation between

TABLE II
MEAN $\pm$ SD OF $\mathcal{E}^v_{\mathrm{M}}(i)$ FOR EACH STUDIED SNR VALUE

SNR (dB)	$\mathcal{E}^v_{\mathrm{SL}}$ (ms)	$\mathcal{E}^v_{\mathrm{SLR}}$ (ms)	$\mathcal{E}^v_{\mathrm{ML}}$ (ms)
30	-5.60 ± 4.3	-0.22 ± 3.9	-0.94 ± 1.9
25	-5.58 ± 4.3	-0.26 ± 3.9	-1.02 ± 1.9
20	-5.58 ± 4.3	-0.16 ± 4.0	-1.08 ± 2.4
15	-5.62 ± 4.2	-0.04 ± 4.2	-1.20 ± 2.5
10	-5.58 ± 4.1	-0.12 ± 4.6	-0.90 ± 2.5

$F_r = 0.27$ Hz, $\phi = 15^{\mathrm{o}}$.

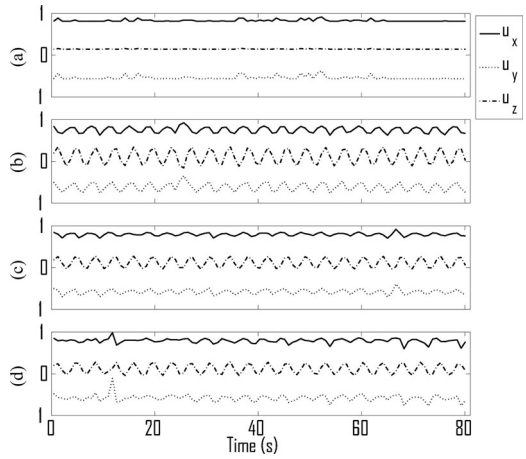

Fig. 9. Main directions $\mathbf{u} = [\mathrm{u}_x, \mathrm{u}_y, \mathrm{u}_z]^T$ of EHV variations found by ML for T_e delineation over: (a) clean simulated signal, (b) simulated signal including respiratory effect, with (c) noise for $\mathrm{SNR} = 30$ dB and (d) noise for $\mathrm{SNR} = 10$ dB.

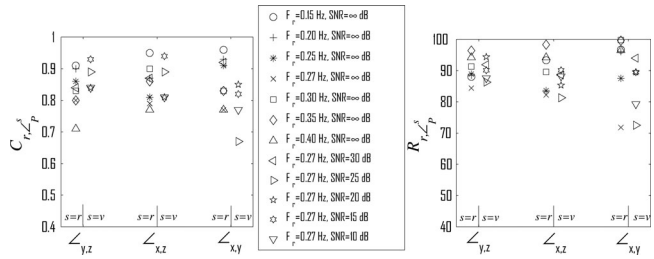

Fig. 10. Linear relation between $r(n)$ and $\angle^s_\rho(n)$: average coherence values and relative fractions of explained variability. (a) $r(n)$ and $\angle^r_\rho(n)$.

$\Delta T_e(i)$ and $\varphi_x(i)$ is found by both methods. Also, $RT^{\mathrm{SLR}}_e(i)$ seems more related with the $\varphi_x(i)$ than $RT^{\mathrm{ML}}_e(i)$. The difference was found to be significatively higher using a unilateral sign test ($p < 0.001$) both for $C_{r,d}$ and $R_{\xi|r}$. The results obtained with $\varphi_y(i)$ and $\varphi_z(i)$ are analogous.

For CDB database recordings, both the linear relation between the (recorded or estimated by rotation angles) respiration with $RT^{\mathrm{M}}_e(i)$ or $\Delta T_e(i)$ are shown in the Fig. 12. Again, a strong relation between $\Delta T_e(i)$ and $\varphi_x(i)$ or $r(n)$ can be observed. The values found by both the methods for the linear relation between $RT^{\mathrm{SLR}}_e(i)$ and $\varphi_x(i)$ compared with $RT^{\mathrm{ML}}_e(i)$ are significatively higher, with all p-values < 0.05 for the unilateral sign. The results obtained with $\varphi_z(i)$ are analogous, while for $\varphi_y(i)$ non significant differences were found.

The linear relation between the *final* direction $\mathbf{u}$ angles and $\varphi_x(i)$ found over PTB database recordings are shown in Fig. 13

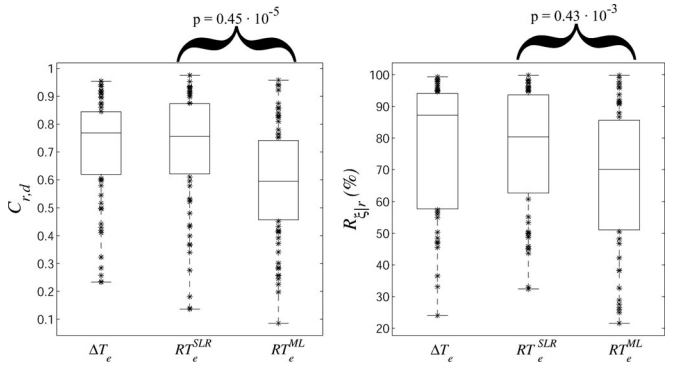

Fig. 11. Results in the PTB database: average coherence values $C_{r,d}$ distribution of $\varphi_x(i)$ with $\Delta T_e(i)$, $RT_e^{\mathrm{SLR}}(i)$, and $RT_e^{\mathrm{ML}}(i)$ series and distribution of relative fraction of $\Delta T_e(i)$, $RT_e^{\mathrm{SLR}}(i)$, and $RT_e^{\mathrm{ML}}(i)$ variability explained by $\varphi_x(i)$. *p*-values unilateral sign test are also indicated.

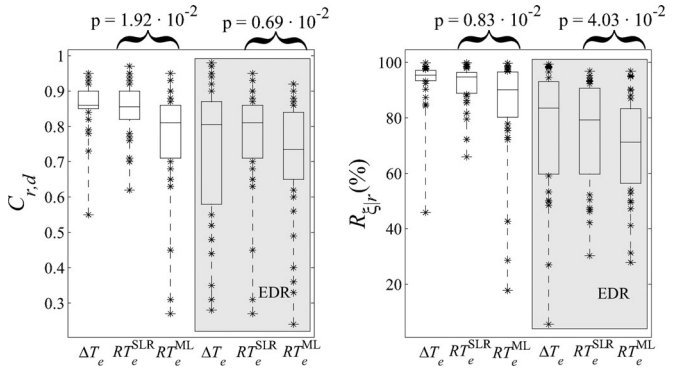

Fig. 12. Results in the CDB: average coherence values $C_{r,d}$ distribution of respiration with $\Delta T_e(i)$, $RT_e^{\mathrm{SLR}}(i)$ and $RT_e^{\mathrm{ML}}(i)$ series and distribution of relative fraction of $\Delta T_e(i)$, $RT_e^{\mathrm{SLR}}(i)$ and $RT_e^{\mathrm{ML}}(i)$ variability explained by respiration, both with respect to recorded and estimated (inside the rectangle) respiration. *p*-values unilateral sign test are also indicated.

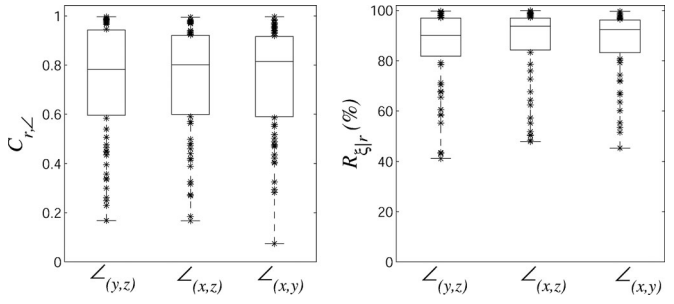

Fig. 13. Values in the PTB database (a) average coherence values distribution of $\varphi_x(i)$ with the *final* direction $\mathbf{u}$ angle series with respect to the (x, y), (x, z), and (y, z) planes. (b) Distribution of relative fraction of $\angle_\rho^r$ variability explained by $\varphi_x(i)$.

while in Fig. 14 the results over CDB recordings are shown, considering both $\varphi_x(i)$ and recorded respiration. High values are typically found, specially with respect to recorded respiration.

IV. Discussion

The delineation approaches used in this paper were previously validated and their performance level has been established elsewhere [18], [19]. In clean simulated data we found a delineation

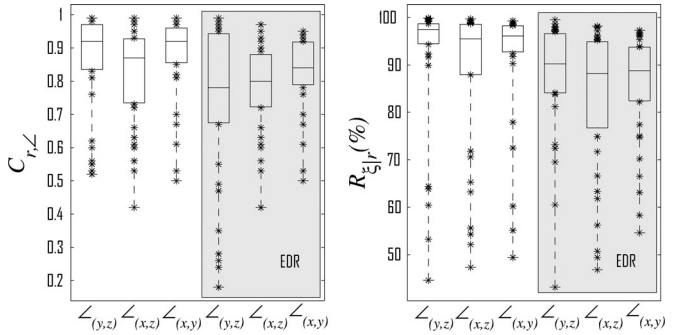

Fig. 14. Values in the CDB (a) average coherence values distribution of recorded and estimated (inside the rectangle) respiration with the *final* direction $\mathbf{u}$ angle series respect to (x, y), (x, z), and (y, z) planes. (b) Distribution of relative fraction of $\angle_\rho^r$ variability explained by respiration.

error for T-wave end with a very low SD for all methods (lower than 2 ms, corresponding to one sample, for SL and ML), but a remarkable bias was found (Table I, last row). The bias using SLR methods is explained by the rule used, favoring the later marks among the 12 leads, and by a reference mark based in three leads only. The huge SL bias is explained by the fact that it was based in the *X*-lead while the T-wave end in the template is taken as the latest SL-based mark, which happen to be the *Y*-lead mark. We recall that $T_e^{\mathrm{ref}}(i)$ are fully determined by the RR and QT series used in the simulation and by the reference marks in the template beat. If SL based is on lead *Z*, instead of lead *X*, equivalent results are obtained (-25.5 ± 1.2), while if lead *Y* is considered a much lower bias is found (0.86 ± 1.1).

The known mechanical effect of respiration which causes ECG morphologic changes morphological is expected to have some influence over the results of automatic delineation, as it has over other indexes [16]. Including mechanical respiration effect, both bias and SD of delineation errors increase and using SL approach one can see a quite remarkable relation between the respiratory signal and both the delineation error and the additional error due to respiration. The additional delineation error caused by the respiration not only contributes for the global delineation error, but it also presents a high dispersion. Thus, the respiratory mechanical influence can contribute for the spurious variability of the T-end mark location. Nevertheless, this additional error is lower using ML delineation, as result of a correct adjustment of the projected leads, with equivalent results found for different respiratory frequencies and noise levels.

The respiration effect was simulated using a sinusoidal signal, which does take into account inspiration/expiration asymmetries. While a more realistic nonsymmetric sigmoidal signal could be used instead, we believe that the rotation resulting from the respiration would not influence differently T-end delineation during inspiration and expiration. The respiratory frequencies considered were limited to the classical range located in the high-frequency band as defined by [25], and similar effects can be expected in the presence of lower respiratory frequencies.

In real data, it was observed that the RT interval typically presents a strong linear relation with respiration (estimated or recorded). This dependency has two possible sources: 1) the mechanical effect of respiration on the ECG waveforms, and 2) the

well-known physiological dependency of RT interval from RR interval and, consequently, from respiration through HR. That relation is higher when compared with recorded respiration, which can result from the fact that the EDR signal, estimated as the rotation angles in the cardiac electrical axis, even though representing a good estimation of periodicity of the respiratory signal, is not linearly related with the air volume in the lungs, in contrast to the respiratory signal recorded by the pressure transducer. The RT interval measure based on SLR T_e location was also found to be significantly more related to respiration (estimated or recorded) than using ML. The only case of non-significance is using the EDR signal estimated from the rotations around lead $y(n)$. Reviewing the EDR signals we found out a signal quite different from the equivalent ones extracted from other leads. Possibly the extraction of the respiration is giving much error on that particular lead as result of the noise. It can be deduced that the high relation of the $\Delta T_e(i)$ with respiration is mainly due to the respiratory influence on SLR marks.

Both in simulated and real data a strong relation between respiratory signals and the angles of the *final* direction $\mathbf{u}$ was found, confirming our hypothesis that ML is adapting the search for the best lead to mark T_e to the respiration-induced changes in the EHV, canceling out the ECG morphologic variations. Both results over simulated and real data allowed us to conclude that the ML allows us to locate T_e more robustly, avoiding the undesirable effect of the mechanically driven respiration-induced variations.

Conclusion

The results obtained in this study confirm the importance of multilead delineation. From comparison between the multilead strategies in both simulated and real signals, a lower influence of the mechanical effect of the respiration on the T_e mark location was observed with ML delineation. The differences between the T_e measures obtained with both ML and SLR are dominated by the mechanical influence of respiration on the SLR mark. In addition, we found out that the selected direction of projection $\mathbf{u}$ in the ML system follows the changes of the cardiac electrical axis caused by respiration, compensating their effect on the T_e mark. Thus, the increased stability in the T_e mark in the ML system with respect to SLR can be explained by a reduction of the variability associated with the mechanical effect of respiration on the delineation. These results lead us to state that for for QT variability analysis, in cardiac risk stratification or drug safety studies, it is highly advisable to use ML delineation strategies.

Appendix

Acronyms and Notation

ANS	Autonomic nervous system.
EDR	ECG-derived respiratory signal.
EHV	Electric heart vector.
ML	Multilead delineation system.
SL	Single-lead delineation system.
SLR	Postprocessing rules after the SL-based delineation.
VCG	Vectorcardiogram.
WT	Wavelet transform.
$C_{r,\mathcal{E}^s_{\mathrm{M}}}$	Average value in a respiratory frequency centered window of the spectral coherence of respiratory signal with $\mathcal{E}^s_{\mathrm{M}}(n)$.
$C_{r,\angle^s_\rho}$	Average value in a respiratory frequency centered window of the spectral coherence between the respiratory signal and the $\angle^s_\rho(i)$.
$e^s_{\mathrm{M}}(i)$	Delineation error for the ith beat by automatic delineation using $M \in \{\mathrm{SL}, \mathrm{SLR}, \mathrm{ML}\}$ approach over the clean ECG ($s \in \{c\}$), ECG with respiration affected ($s \in \{r\}$), and ECG with noise contamination ($s \in \{v\}$).
RT^M_e	Time interval measured from the R peak obtained with SLR to T_e obtained with each delineation approach $M \in \{\mathrm{SLR}, \mathrm{ML}\}$.
$R^s_{\xi\|r}$	Relative fraction of $\mathcal{E}^s_{\mathrm{M}}(i)$ HF variability explained by the respiration, where $s \in \{r, v\}$ stands for ECG with respiration simulated effect and with noise contamination, respectively.
$r(n)$	Respiratory signal.
T_e	T wave end.
$T^{\mathrm{ref}}_e(i)$	Reference T_e location for the ith beat
$\mathbf{u}$	Main direction of EHV variations.
$T^{\mathrm{M,s}}_e(i)$	T_e mark for the ith beat obtained by automatic delineation using $M \in \{\mathrm{SL}, \mathrm{SLR}, \mathrm{ML}\}$ approach over the clean ECG ($s \in \{c\}$), ECG with respiration simulated effect ($s \in \{r\}$), or ECG with noise contamination ($s \in \{v\}$)
$w_{s,m}(n)$	WT of a signal $s(n)$ in the scale m.
$\mathbf{w}_m(n)$	WT loop in the scale m.
$\mathcal{E}^s_{\mathrm{M}}(i)$	Additional error for the ith beat due to respiration or noise ($s \in \{r, v\}$) with respect to the automatic location over the clean signal $T^{\mathrm{M,c}}_e(i)$.
$\angle^s_\rho(i)$	Angles of $\mathbf{u}$ for the ith beat with respect to the plane defined by each pair of orthogonal leads $\rho \in \{(x,y),(y,z),(x,z)\}$, $s \in \{r, v\}$ $\angle^s_\rho(n)$.
$\Delta T_e(i)$	Differences between the automatic T_e location on beat i obtained using ML and SLR delineation approaches.
$\varphi_x(i), \varphi_y(i)$ and $\varphi_z(i)$	Series of rotation angles around each orthogonal lead estimated with the EDR algorithm.

References

[1] L. Sörnmo and P. Laguna, *Bioelectrical Signal Processing in Cardiac and Neurological Applications*, New York: Elsevier, 2005.

[2] M. Malik and A. J. Camm, *Dynamic Electrocardiography*. Oxford: Blackwell, 2004.

[3] R. Almeida, J. P. Martínez, A. P. Rocha, S. Olmos, and P. Laguna, "Improved QT variability quantification by multilead automatic delineation," in *Computers in Cardiology 2005*, vol. 32. Washington, DC: IEEE Computer Society Press, pp. 503–506, 2005.

[4] A. Porta, G. Baselli, E. Caiani, A. Malliani, F. Lombardi, and S. Cerutti, "Quantifying electrocardiogram RT-RR variability interactions," *Med. Biol. Eng. Comput.*, vol. 36, pp. 27–34, 1998.

[5] J. P. Couderc and C. M. lopes, "Short and long QT syndromes: Does QT length really matter?" *J. Electrocardiol.*, vol. 43, no. 5, pp. 396–399, 2010.

[6] D. J. Whellan, C. L. Green, J. P. Piccini, and M. W. Krucoff, "QT as a safety biomarker in drug development," *Clin. Pharmacol. Therapeut.*, vol. 36, no. 1, pp. 101–104, 2009.
[7] J. P. Piccini, D. J. Whellan, B. R. Berridge, J. K. Finkle, S. D. Pettit, N. Stockbridge, J. P. Valentin, H. M. Vargas, and M. W. Krucoff, "Current challenges in the evaluation of cardiac safety during drug development: Translational medicine meets the critical path initiative," *Amer. Heart J.*, vol. 158, no. 3, pp. 317–326, 2009.
[8] E. Pueyo, J. P. Martínez, and P. Laguna, "Cardiac repolarisation analysis using the surface ECG," *Philos. Trans. R. Soc.—A*, vol. 367, pp. 213–233, 2009.
[9] C. P. Dobson, M. T. La Rovere, C. Olsen, M. Berardinangeli, M. Veniani, P. Midi, L. Tavazzi, M. Haigney, and on behalf of the GISSI-HF Investigators, "24-Hour QT variability in heart failure," *J. Electrocardiol.*, vol. 42, no. 6, pp. 500–504, 2009.
[10] M. Hinterseer, B. M. Beckmann, M. B. Thomsen, A. Pfeufer, M. Ulbrich, M. F. Sinner, S. Perz, H. E. Wichmann, C. Lengyel, R. Schimpf, S. K. Maier, A. Varró, M. A. Vos, G. Steinbeck, and S. Kääb, "Usefulness of short-term variability of QT intervals as a predictor for electrical remodeling and proarrhythmia in patients with nonischemic heart failure," *Amer. J. Cardiol.*, vol. 106, no. 2, pp. 216–220, 2010.
[11] J. Malmivuo and R. Plonsey, *Bioelectromagnetism—Principles and Applications of Bioelectric and Biomagnetic Fields*. London: Oxford Univ. Press, 1995.
[12] M. Malik, "Beat-to-beat QT variability and cardiac autonomic regulation," *Amer. J. Physiol. Heart Circ. Physiol.*, vol. 295, no. 3, pp. H923–H925, Sep. 2008.
[13] J. Flaherty, S. D. Blumenschen, A. W. Alexander, R. D. Gentzler, T. M. Gallie, J. P Boineau, and M. S. Spach, "Influence of respiration on recording cardiac potentials," *Amer. J. Cardiol.*, vol. 20, pp. 21–28, 1967.
[14] M. Aström, H. C. Santos, L. Sörnmo, P. Laguna, and B. Wohlfart, "Vectorcardiographic loop alignment and the measurement of morphologic beat-to-beat variability in noisy signals," *IEEE Trans. Biomed. Eng.*, vol. 47, no. 4, pp. 497–506, Apr. 2000.
[15] F. Yasuma and J. Hayano, "Respiratory sinus arrhythmia. Why does the heartbeat synchronize with respiratory rhythm?," *Chest*, vol. 125, pp. 683–690, 2004.
[16] L. Sörnmo, "Vectorcardiographic loop alignment and morphologic beat-to-beat variability," *IEEE Trans. Biomed. Eng.*, vol. 45, no. 2, pp. 1401–1413, Dec. 1998.
[17] M. Noriega, R. Almeida, J. P. Martínez, and P. Laguna, "Medida Multiderivacional de QT en el ECG de 12 derivaciones del sistema EASI," presented at the 27th Congreso Anual de la Sociedad Española de Ingeniería Biomédica, Cádiz, España, Nov. 18–20, 2009.
[18] J. P. Martínez, R. Almeida, S. Olmos, A. P. Rocha, and P. Laguna "Wavelet-based ECG delineator: Evaluation on standard databases," *IEEE Trans. Biomed. Eng.*, vol 51, no. 4, pp 570–581, Apr. 2004.
[19] R. Almeida, J. P. Martínez, A. P. Rocha, and P. Laguna, "Multilead ECG delineation using spatially projected leads from wavelet transform loops," *IEEE Trans. Biomed. Eng.*, vol. 56, no. 8, pp. 1996–2005, Aug. 2009.
[20] The CSE Working Party, "Recommendations for measurement standards in quantitative electrocardiography," *Eur. Heart J.*, vol. 6, pp. 815–825, 1985.
[21] P. Laguna, R. Jané, and P. Camina, "Automatic detection of wave boundaries in multilead ECG signals: Validation with the CSE database," *Comput. Biomed. Res.*, vol. 27, no. 1, pp. 45–60, Feb. 1994.
[22] S. Mallat and S. Zhong, "Characterization of signals from multiscale edge," *IEEE Trans. Pattern Anal. Mach. Intell.*, vol. 14, no. 7, pp. 710–732, Jul. 1992.
[23] I. Christov, I. Otsinsky, I. Simova, R. Prokopova, E. Trendafilova, and S. Naydenov, "Dataset of manually measured QT intervals in the electrocardiogram," *Biomed. Eng. Online* vol. 31, no. 5, pp. 5–31, 2006.
[24] G. E. Dower, "The ECGD: A derivation of the ECG from VCG leads," *J. Electrocardiol.*, vol. 17, no. 2, pp. 189–191, 1984.
[25] Task Force of The ESC/ASPE, 1996, "Heart rate variability: Standards of measurement, physiological interpretation, and clinical use," *Eur. Heart J.*, vol. 17, pp. 354–381, 1996.
[26] R. Bailón, L. Sörnmo, and P. Laguna, "A robust method for ECG-based estimation of the respiratory frequency during stress testing," *IEEE Trans. Biomed. Eng.*, vol. 53, no. 7, pp. 1273–1285, Jul. 2006.
[27] R. Bailón, J. Mateo, S. Olmos, P. Serrano, J. García, A. del Río, I. Ferreira, and P. Laguna, "Coronary artery disease diagnosis based on exercise electrocardiogram indexes from repolarisation, depolarisation and heart rate variability," *Med. Biol. Eng. Comput.*, vol. 41, pp. 561–571, 2003.
[28] T. Soderstrom, "Convergence properties of the generalised least squares identification method," *Automatica*, vol. 10, pp. 617–626, 1974.

Maikel Noriega received the M.S. degree in telecommunications and electronic engineering from the University of Oriente, Santiago de Cuba, Cuba, and the Master's degree in biomedical engineering from the University of Zaragoza, Zaragoza, Spain, in 2004 and 2010, respectively, where he is currently working toward the Ph.D. degree in the field of biomedical signal processing.

He is currently an Assistant Professor of Communications Theory in the Department of Telecommunications Engineering, University of Oriente, Santiago de Cuba, Cuba. Since 2008, he has been a Researcher at the Aragón Institute of Engineering Research, Zaragoza. His current research interests include biomedical signal processing, especially focused on the wavelet-based methods for automatic delineation of the ECG.

Juan Pablo Martínez was born in Zaragoza, Spain, in 1976. He received the M.S. degree in telecommunication engineering and the Ph.D. degree in biomedical engineering from the University of Zaragoza (UZ), Zaragoza, in 1999 and 2005, respectively.

Since 2000, he has been an Assistant Professor at the Aragon Institute of Engineering Research, UZ, where he has been an Associate Professor since 2007. He is also with the Centro de Investigación Biomedica en Red en Bioingeniéria, Biomateriales y Nanomedicina, Zaragoza. His current research interests include biomedical signal processing, with main interest in signals of cardiovascular origin.

Pablo Laguna (M'92–SM'06) was born in Jaca (Huesca), Spain, in 1962. He received the M.S. degree in physics and the Ph.D. degree in physic science from the Science Faculty, University of Zaragoza, Zaragoza, Spain, in 1985 and 1990, respectively. The Ph.D. thesis was developed at the Biomedical Engineering Division of the Institute of Cybernetics (U.P.C.-C.S.I.C.) under the direction of P. Caminal.

He is currently a Full Professor of Signal Processing and Communications in the Department of Electrical Engineering, Engineering School, where he has being vice-dean for international relation (1999–2002), and a researcher at the Aragón Institute for Engineering Research (I3A), both at University of Zaragoza, Spain, where he has being responsible of the Biomedical Engineering division of the I3A (2000–2011) and of the Biomedical Engineering Master (2003–2010). His professional research interests are in Signal Processing, in particular applied to Biomedical applications. He has co-authored more than 80 research papers on this topic, over 200 international conference papers, and has advise 10 Ph.D. Thesis. He has lead a broad number of projects on biomedical signal interpretation specially in the cardiovascular domain, most of them with international collaborations at clinical and engineering sites. He is having some international scientific responsibilities, as serving at the board of Computing in Cardiology conference, editor of the *Digital Signal Processing* Journal (Eurasip), and of the *Journal of Electrocardiology*, organizer of different scientific conferences, etc. He is also member, and currently director, of the Spanish Center for Biomedical Engineering, Biomaterial and Nano-medicine Research CIBER-BBN, and responsible of the Ph.D. program in Biomedical Engineering at Zaragoza University. He is, together with L. Sörnmo, the author of the *Bioelectrical Signal Processing in Cardiac and Neurological Applications* (Amsterdam: Elsevier, 2005). His professional research interests include signal processing, in particular applied to biomedical applications.

Raquel Bailón was born in Zaragoza, Spain, in 1978. She received the M.Sc. degree in telecommunication engineering and the Ph.D. degree in biomedical engineering from the University of Zaragoza (UZ), Zaragoza, in 2001 and 2006, respectively.

She was an Assistant Professor with the Department of Electronic Engineering and Communications, UZ, from 2003 to 2010, where she is an Associate Professor since 2010. She is also a Researcher with the Aragón Institute for Engineering Research, Zaragoza, and also with the Biomedical Research Networking Center in bioengineering, biomaterials and nanomedicine, Zaragoza. Her current research interests include the biomedical signal processing field, specially in the analysis of the dynamics and interactions of cardiovascular signals.

Rute Almeida was born in Porto, Portugal in 1979. She received a 4 years degree in mathematics applied to technology in 2000 and the European Doctor Degree (Ph.D. in applied mathematics) in 2007 from Faculty of Sciences, University of Porto (FCUP), Oporto, Portugal.

She was with the Autonomic Function Study Center from Hospital S. João from March to October 2001, working in methods for automatic delineation of the ECG. She was supported by an individual grant from the Foundation for Science and Technology (Portugal) and the European Social Fund, from October 2001 to September 2005. Since 2005, she is a member of the Centro de Matemática da Universidade do Porto (CMUP), Porto, Portugal.

From June 2007 to June 2012, she was a researcher at the Spanish center for Biomedical Engineering, Biomaterial and Nano-medicine Research CIBER-BBN (Centro de Investigación Biomédica en Red en Bioingeniería, Biomateriales y Nanomedicina), under protocol with the University of Zaragoza (UNIZAR), Zaragoza, Spain. She was also with the Aragón Institute for Engineering Research (I3A) at UNIZAR. Since July 2012, she is a postdoctoral researcher at CMUP, Porto, Portugal.